ACS APPLIED MATERIALS & INTERFACES

www.acsami.org

Research Article

On the Colloidal Stability of PbS Quantum Dots Capped with Methylammonium Lead Iodide Ligands

Dmytro Bederak, Nataliia Sukharevska, Simon Kahmann, Mustapha Abdu-Aguye, Herman Duim, Dmitry N. Dirin, Maksym V. Kovalenko, Giuseppe Portale, and Maria A. Loi*

Cite This: *ACS Appl. Mater. Interfaces* 2020, 12, 52959–52966

Read Online

ACCESS | Metrics & More | Article Recommendations | Supporting Information

ABSTRACT: Phase-transfer exchange of pristine organic ligands for inorganic ones is essential for the integration of colloidal quantum dots (CQDs) in optoelectronic devices. This method results in a colloidal dispersion (ink) which can be directly deposited by various solution-processable techniques to fabricate conductive films. For PbS CQDs capped with methylammonium lead iodide ligands ($MAPbI_3$), the most commonly employed solvent is butylamine, which enables only a short-term (hours) colloidal stability and thus brings concerns on the possibility of manufacturing CQD devices on a large scale in a reproducible manner. In this work, we studied the stability of alternative inks in two highly polar solvents which impart long-term colloidal stability of CQDs: propylene carbonate (PC) and 2,6-difluoropyridine (DFP). The aging and the loss of the ink's stability were monitored with optical, structural, and transport measurements. With these solvents, PbS CQDs capped with $MAPbI_3$ ligands retain colloidal stability for more than 20 months, both in dilute and concentrated dispersions. After 17 months of ink storage, transistors with a maximum linear mobility for electrons of 8.5×10^{-3} cm^2/V s are fabricated; this value is 17% of the one obtained with fresh solutions. Our results show that both PC- and DFP-based PbS CQD inks offer the needed shelf life to allow for the development of a CQD device technology.

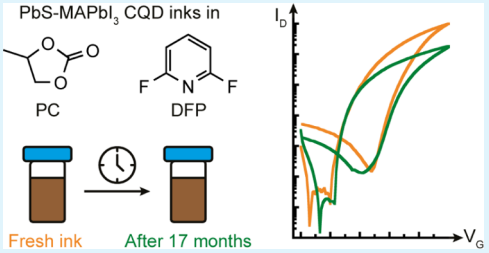

KEYWORDS: *colloidal quantum dots, lead sulfide, inks, stability, $MAPbI_3$*

INTRODUCTION

Colloidal quantum dots (CQDs) have been in research spotlight over the last few decades as versatile building blocks for the fabrication of optoelectronic devices. PbS CQDs are among the most studied and promising members of this family of semiconductors due to their large exciton Bohr radius and dielectric permittivity, size-tunable band gap ranging from the near-infrared to the visible spectral region, high compliance with modification of the surface chemistry, and their relatively high stability in ambient conditions.[1] PbS CQDs are successfully employed in solar cells,[2] light-emitting diodes,[3] light-emitting transistors,[4,5] inverters,[6] and photodetectors.[7] For many years, one of the limiting steps in the fabrication of CQD devices has been the exchange of ligands in solid films which required layer-by-layer processing.[8] In the last 12 years, the so-called phase-transfer ligand exchange (PTLE) has been adopted for small inorganic ligands,[9,10] namely chalcogenides and metal chalcogenide complexes, pseudohalides, halides, and halometallate complexes.[11−17]

PTLE results in a solution of ligand-exchanged CQDs (so-called inks), which can be used for the deposition of conductive CQD films by various deposition techniques, such as spin-coating, blade-coating, slot-die coating, dip-coating, and spray-coating. Much of the research performed in the last years on CQD solar cells employed sub-micrometer layers of iodide-capped PbS CQDs, wherein a solid-state ligand exchange of initial long-chain organic ligands with tetrabutylammonium iodide was carried out. Fabrication of such solar cells involved the deposition of up to 12 layers, each requiring at least 3 steps.[18,19] Multiple depositions by spin-coating are extremely wasteful since most of the ink is lost. Nowadays, the most efficient PbS CQD solar cells are fabricated by depositing a single layer of CQDs capped with lead halides or haloplumbate complexes.[2] While the fabrication time and costs are considered as the main advantages of the ink deposition compared to the layer-by-layer approach with solid-state ligand exchange, the ink preparation itself requires a large investment of time and materials accounting for up to 50% of the production cost for a device-ready ink based on PbS CQDs.[20] A severe problem arises given that the shelf time of the most popular inks which employ butylamine as a solvent lies below a few hours. Butylamine plays a double role in such inks: it is not only the solvent, but it also re-caps negatively charged CQDs as the butylammonium cation, which is formed *in situ* by reaction with the methylammonium counterion. Such

Received: September 15, 2020
Accepted: November 2, 2020
Published: November 11, 2020

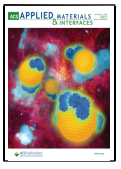

CQDs are colloidally stabilized by steric repulsion of butylammonium chains, which can be easily removed from the deposited film by mild annealing, as butylamine has a low boiling point (78 °C). This allows to obtain good quality CQD layers with conventional deposition methods such as spin-coating. For this reason, a majority of the latest reports on PbS CQD solar cells use butylamine as a solvent.[21,22] However, as a short-chain ligand, butylammonium cannot enable long-term colloidal stability of the PbS CQDs.[23,24] A few strategies to improve the colloidal stability of butylamine-based inks have been recently proposed. These strategies include the addition of longer-chain amines to enhance steric repulsion[23] or addition of 3-mercaptopropionic acid ligands to the lead halide-capped CQDs.[24] The latter approach, which was reported during the preparation of this manuscript, substantially improves the long-term stability of the inks resulting in over 2 months of shelf time. However, no systematic investigation of aging of these or other inks has hitherto been reported. Highly stable ligand-exchanged CQD inks will be the next milestone for further industrialization of CQD-based technologies.

In this work, the stability of PbS CQDs capped with methylammonium lead iodide ligands ($MAPbI_3$) was investigated. After ligand exchange, PbS-$MAPbI_3$ CQDs were dispersed in either propylene carbonate (PC) or 2,6-difluoropyridine (DFP) forming highly stable inks. The long-term evolution of the optical properties of the inks was monitored by means of absorption and photoluminescence (PL) spectroscopy. The position of the first excitonic peak and the optical density were stable for over 80 days. Careful analysis of the emission spectra showed the appearance of a low-energy emission peak, which becomes dominant after a year of storage. This peak indicates aggregation in solution, which is confirmed by small-angle X-ray scattering (SAXS) analysis showing the presence of chain-like branched CQD aggregates in the inks. Nevertheless, the inks retain their overall colloidal stability and can be used to fabricate well-performing devices for more than 17 months.

RESULTS AND DISCUSSION

In this work, two polar solvents, namely PC and DFP, were used for the redispersion of the ligand-exchanged CQDs. PC was chosen due to its high static dielectric constant (ε = 62.9) and its previous use for efficient electrostatic stabilization of colloidal inks.[14,25] One of the main drawbacks of PC as a solvent is its high boiling point (T_{bp} = 242 °C), which requires heating to facilitate the drying process during the film deposition. DFP also possesses a high dielectric constant (ε = 107.8) but has a relatively low boiling point (T_{bp} = 124 °C), rather unusual for highly polar organic solvents.[26] The relationship between the dielectric constant and boiling point of the organic solvents used for the ink preparation is illustrated in Figure S1. Highly polar solvents like formamide and N-methylformamide (NMF) do not form stable colloidal inks due to strong anion desorption, while polar solvents with relatively low dielectric constant [like dimethylformamide (DMF)] can even be used as a nonsolvent for PbS CQDs capped with lead halide ligands.[14] Overall, the unique combination of the abovementioned parameters makes DFP one of the most promising solvents for CQD inks. DFP has been recently introduced as a solvent for lead chalcogenide CQD inks with (pseudo)halides and metal halide ligands, but halometallate complexes were not included in this earlier study.[27] In this work, PbS CQDs capped with the model $MAPbI_3$ ligands were prepared and dispersed in either PC or DFP at the desired concentration (see the Experimental Section for more details). $MAPbI_3$ ligands were chosen for this study because they provide good passivation of the PbS CQD surface. Furthermore, PbS-$MAPbI_3$ were used for fabrication of highly efficient PbS CQD solar cells.[28,29] The schematic route of the ligand exchange is shown in Figure 1A.

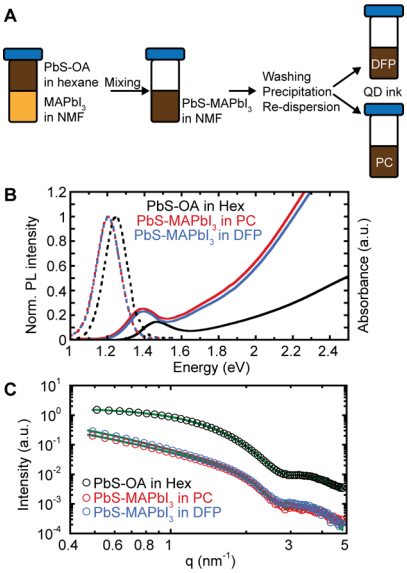

Figure 1. (A) Schematic illustration of CQD ink preparation. (B) Absorption spectra (solid lines) of PbS CQDs capped with native OA ligands in hexane (black) and of PbS CQDs capped with $MAPbI_3$ either in PC (red) or in DFP (blue). PL spectra of these dispersions are shown by dashed lines. (C) SAXS curves for the CQD native solution and the inks in PC and DFP. Green lines are best fit curves.

Absorption and PL spectra of PbS CQDs with native oleic acid (OA) and $MAPbI_3$ ligands are shown in Figure 1B. The extracted peak positions, values of full width at half-maximum (fwhm), and Stokes shift are summarized in Table 1. The first excitonic peak in the absorption spectrum of oleate-capped PbS CQDs lies at 1.47 eV. It slightly red-shifts (<0.07 eV) after the ligand exchange with $MAPbI_3$ and redispersion in polar solvents, which is typically assigned to the difference in dielectric permittivity of solvents, as well as, to a lowering of the quantum confinement in case of the CQDs capped with $MAPbI_3$ ligands. The PL spectra of these dispersions show a similar trend. The emission of the ligand-exchanged CQDs is red-shifted by 0.04 eV compared to the emission of the PbS-OA dispersion, which is in agreement with the literature.[30] The width of the first excitonic peak both in the absorption and PL spectra is preserved, which indicates that the ligand exchange does not induce significant changes in the size distribution of CQDs or other sources of energetic disorder. The Stokes shift of the inks is slightly smaller than the one of the oleate-capped PbS CQDs, while an opposite trend was observed previously.[30] Possible reasons for this discrepancy could be the slightly different size of PbS CQDs used before or differences in ligand exchange protocols, for example much longer ligand-exchange time (12−24 h) and extra waiting time of 1−2 h to settle the CQDs before centrifugation, which were not needed in our case.

https://dx.doi.org/10.1021/acsami.0c16646
ACS Appl. Mater. Interfaces 2020, 12, 52959−52966

Table 1. Absorption and Emission Peak Positions, fwhm, and Stokes Shift of the Oleate-Capped PbS in Hexane and PbS-$MAPbI_3$ in PC and DFP

sample	absorption, eV	fwhm of absorption, eV	emission, eV	fwhm of emission, eV	Stokes shift, meV
PbS-OA in Hex	1.47	0.26	1.25	0.21	224
PbS-$MAPbI_3$ in PC	1.40	0.28	1.21	0.21	191
PbS-$MAPbI_3$ in DFP	1.40	0.28	1.20	0.22	197

Time-resolved PL measurements reveal long PL lifetimes for all three samples, which indicates good surface passivation of pristine and ligand-exchanged CQDs. The oleate-capped CQDs show a lifetime of 2.7 μs, while the lifetime of $MAPbI_3$-capped CQDs dispersed in PC and DFP is 3.2 and 2.9 μs, respectively (the PL decay is shown in Figure S2). We note that the lifetimes are also affected by the high dielectric constant of the solvents.[31]

The size and dispersity of the CQDs in the suspension have been characterized using solution SAXS. SAXS measurements of the CQDs with native OA show good dispersity of the individual particles (see Figure 1C). The presence of a clear minimum at $q \sim 2.87$ nm^{-1} is indicative of low polydisperse particles with an average radius $R = 4.49/2.87 = 1.56$ nm.[32] A more quantitative analysis by modeling of the SAXS intensity using the scattering function for an ensemble of spherical objects was performed. In this case, an average radius of 1.65 nm with Gaussian size polydispersity of width 0.25 nm was obtained and the used model excellently describes the experimental curve (Figure 1C). It should be noted that SAXS is only sensitive to the size of the PbS core but not the ligand shell as the electron density of the inorganic part is much higher than that of OA. Thus, the calculated value is a direct representation of the CQD radius.

Interestingly, the SAXS curves of the freshly prepared CQD inks in PC and DFP show a significant alteration with respect to the PbS-OA dispersed in hexane (see Figure 1C). The SAXS profiles in PC and DFP show a linear trend in the log–log plot for q values <1.4 nm^{-1}, indicative of a power law $q^{-\alpha}$ trend, which can be related to aggregation between particles.[33] The exponent is ~1.8 for PC and ~2 for DFP. Values of α close to 2 represent the fractal dimension D_f of the CQD aggregates and suggest that branched aggregates are present in both solvents.[34] Their formation is probably induced by the ligand exchange. However, the overall size of these colloidal aggregates falls outside of the probed SAXS range. The fact that the intensity minimum position does not shift in q suggests that the subunits of these aggregates are the CQDs with unmodified dimensions.

If we aim to develop a technology with CQD inks, the quality of the surface passivation is one of the important parameters because it determines the overall quality of the transport properties. At the same time, the stability of the inks is as important since it determines how feasible the industrialization of the CQD deposition process is.

Figure 2 (top row) shows pictures of PbS-$MAPbI_3$ dispersions in butylamine, which is one of the most favored solvents for making CQD devices.[29,35,36] When fabricated at high concentrations, PbS-$MAPbI_3$ dispersions in butylamine are typically stable for a few hours (see Figure 2A). After this time frame, agglomerates become visible by eye. Filtering the dispersion and making devices are impossible at this point (Figure 2B). This requires that a new ink in butylamine has to be prepared each time before the fabrication of a new batch of devices and the leftover has to be disposed of. When

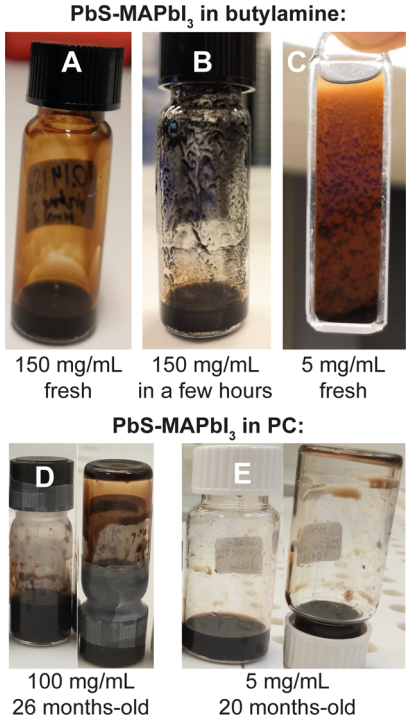

Figure 2. Photographs of the PbS-$MAPbI_3$ inks. (A) As-prepared ink in butylamine of 150 mg/mL concentration. (B) Same solution after a few hours. (C) Cuvette containing a freshly prepared PbS-$MAPbI_3$ ink in butylamine with a concentration of 5 mg/mL. At this concentration, the colloidal stability of the ink in butylamine is lost within 30 min. (D) 26-month-old PbS-$MAPbI_3$ ink in PC of 100 mg/mL concentration in a 4 mL vial. (E) PbS-$MAPbI_3$ in PC of 5 mg/mL concentration stored for 20 months in a 20 mL vial.

dispersions in butylamine are diluted, for example to a 5 mg/mL concentration, swift agglomeration occurs with subsequent settlement of the agglomerates at the bottom of a cuvette (Figure 2C). This rapid degradation of PbS-$MAPbI_3$ inks in butylamine can be tracked by a significant red-shift of the PL peak (Figure S7). A very different case is shown in the bottom row of Figure 2, where PbS-$MAPbI_3$ inks in PC both at high and low concentrations retain colloidal stability after 27 and 20 months, respectively.

The colloidal stability of PbS-$MAPbI_3$ dispersions in PC and DFP was monitored through their absorption and PL spectra. The evolution of the first excitonic peak position in absorption and the corresponding optical density are shown in Figure 3A. The spectra themselves are presented in Figure S4. Both parameters remain constant for 80 days, indicating the high colloidal stability of the inks and the absence of Ostwald ripening or strong coagulation in the samples. The peak position in the emission spectra is also unaffected during the same time span (at least 3 months) for both inks (Figure 3B). The lower energy emission shoulder slightly increases over time, and after prolonged ink storage (12 months), the emission peak at 0.95 eV becomes dominant (black curves in

https://dx.doi.org/10.1021/acsami.0c16646
ACS Appl. Mater. Interfaces 2020, 12, 52959−52966

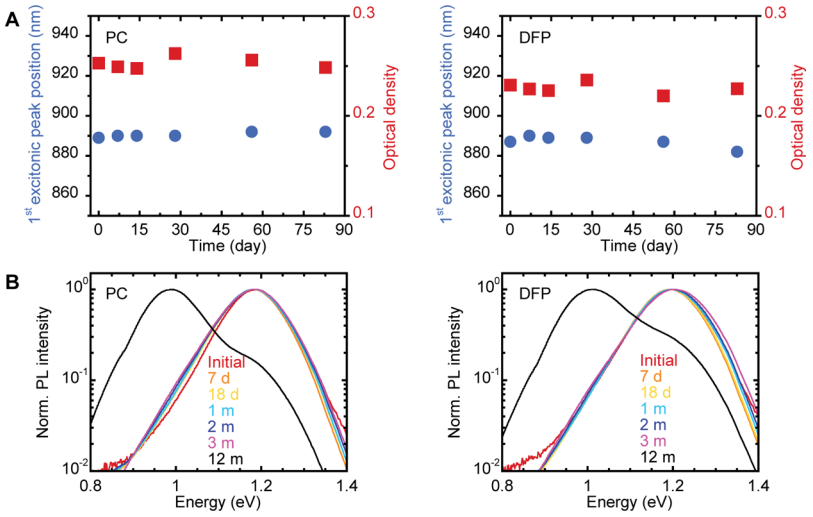

Figure 3. (A) Changes of the first excitonic peak position (blue circles) and optical density corresponding to this peak (red squares) during storage for PbS-MAPbI$_3$ CQDs in PC (left) and in DFP (right). (B) Normalized PL spectra of the same inks. d and m indicate days and months, respectively.

Figure 3B). The PL spectrum of two 18-month-inks in PC (Figure S5) is similar to the one of a year-old ink.

The change of the PL lifetime during the storage can also give important information on the ink quality. Extracted PL lifetimes are shown in Figure S6. The PL lifetime of the inks in PC does not deteriorate over time and even after 18 months of storage, it is still close to the initial 3 μs. The PL lifetime of the inks in DFP initially drops within the first 2 months and then settles above 2 μs which indicates a slight increase of non-radiative decay processes. The large stability of the PL lifetime of the PC sample allows us to speculate on the origin of the increasing PL intensity at 0.95 eV. Generally speaking, such an effect could be due to emissive trap states,[37] for example on the surface, or to partial aggregation and necking of the CQDs,[38] as both phenomena have been discussed in CQD films. However, since the lifetime of the main peak remains unaffected, this is a strong evidence of necking and merging of CQDs into larger size particles. Energy transfer is responsible for making this effect more observable in the PL spectra than in absorption.

The stability of the inks in PC and DFP is further confirmed by the comparison of the SAXS profiles of the fresh and 12 months aged inks (see Figure 4). The SAXS data show no change of the ink structure within the experimental error for the sample in PC. In the case of DFP, a small change in the SAXS curve in the low q-range is detected after 1 year, pointing out to a small rearrangement of the CQD aggregates. However, the effect is small.

In the last sections, we collected substantial evidences of the high stability of the inks in PC and DFP, with superior behavior of the former, as displayed by the stable PL lifetime. To test the effect of the ink aging on electric transport properties of the fabricated films, field-effect transistors (FETs) with fresh and aged inks were fabricated. The transfer characteristics for the FETs prepared with fresh and aged inks in PC are shown in Figure 5. Devices deposited from a fresh ink exhibit electron-dominated ambipolar transport, with electron current 3 orders of magnitude higher than the hole current. The extracted linear mobility for electrons is 5.0 × 10^{-2} cm^2/V s, while the hole mobility was found to be 2.9 × 10^{-5} cm^2/V s, which are consistent with the previously

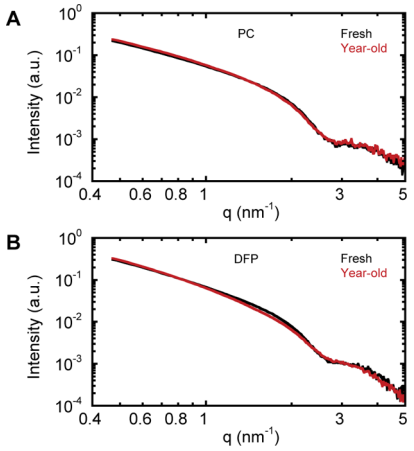

Figure 4. Comparison between the SAXS profiles of the fresh and 12-month-old PbS-MAPbI$_3$ CQD inks in PC (A) and DFP (B).

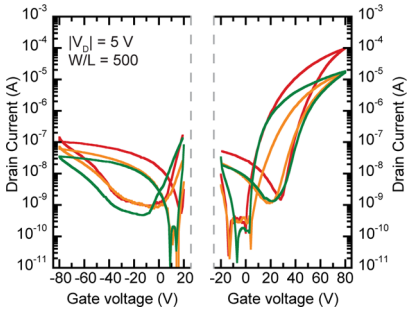

Figure 5. Transfer characteristics of the FETs prepared from the same PbS-MAPbI$_3$ CQD ink in PC at a different storage time. Red line corresponds to the device fabricated with a fresh ink, orange to the 3-month-old ink and green to the 17-month-old ink. It is important to notice that devices produced with 17-month-old ink show a larger variability.

published report on PbS-MAPbI$_3$ FETs after the MeOH washing.[30] Aging of the inks for 3 and 17 months, results in a decrease of both electron and hole currents with preservation of electron-dominated transport. The electron mobility of the devices made with 3-month-old inks in PC is 9.3 × 10^{-3} cm^2/

https://dx.doi.org/10.1021/acsami.0c16646
ACS Appl. Mater. Interfaces 2020, 12, 52959−52966

V s, which is approaching the values for iodide-capped PbS FETs fabricated by solid-state ligand exchange.[18,39] The output characteristics of these FETs are shown in Figure S8. The FETs deposited from a 17-month-old PC ink exhibit an average electron mobility of 5.2×10^{-3} cm^2/V s but with a relatively broad distribution of values (Figure S9). The hysteresis for holes is higher than the one for electrons, which is consistent with previous reports on PbS-$MAPbI_3$ transistors.[30] The presence of the hysteresis in the CQD FETs is typically assigned to the presence of the charge traps either in the CQD film or at the interface between the CQD film and the dielectric layer.[5,40−42] The off-state of the devices is limited by the gate leakage current (Figure S10), which is about 1 nA. The slightly lower performance of the aged inks notwithstanding, these results demonstrate that it is possible to obtain long shelf time for PbS-$MAPbI_3$ CQDs.

The FETs fabricated with fresh DFP-based inks are similar to the devices made from fresh PC inks (Figure S11) showing that the solvent of a colloidal ink does not influence the device performance when the processing conditions can be tuned to the boiling point of the solvents. Here, it is important to underline that the devices were fabricated through blade-coating, which is not only a scalable technique but one that can be adapted easily to high boiling point solvents. The electron current and electron mobility of the DFP-based devices are not affected by the ink aging up to 2 months. The extracted electron mobility for both fresh and for 2-month-old inks is about 5×10^{-2} cm^2/V s, which is comparable to the electron mobility values of the transistor fabricated with the fresh PC-based ink.

As the original CQDs used to prepare our inks are identical, the ink stability depends only on the properties of the solvent. Both PC and DFP have a high dielectric constant which primarily governs the colloidal stability. However, other important parameters for the solvents are their ability to solvate anions and cations. The solvation of anions, in other words the evaluation of the solvent Lewis acidity, can be represented by a normalized Dimroth−Reichardt parameter (E_T^N).[14] For PC, $E_T^N = 0.472$, while for DFP $E_T^N = 0.389$, which makes both of them weak Lewis acids and therefore makes desorption of anionic PbI_3^- species highly unlikely.[43] Solvation of cations arises from the Lewis basicity of the solvents and correlates with the solvent donor number (DN).[14] However, the DN of DPF is not reported in the literature and the Kamlet−Taft β parameter is instead used for the comparison since it correlates with the Gutmann DN values.[44] For DFP, only calculated β_{OH} and β_{NH_2} values are available.[45] Since β_{NH_2} values for pyridines correlate much better with β values, they were chosen for a fair comparison. The β value for PC is 0.40, while for DFP, it is 0.31. This means that DFP may solvate methylammonium cations slightly less efficiently. Furthermore, the Kamlet−Taft β parameter mainly accounts for the ability of a solvent to accept a hydrogen bond,[46] but it does not consider dipolarity/polarizability and steric hindrance of the solvent molecules, both of which play a notable role in solvation.[45] The dipole moment of PC (4.95) is higher compared to DFP (3.74−3.82),[45,47] whereas the nucleophilic groups of PC are more accessible than in DFP (meaning that PC might only be a slightly stronger base but notably stronger nucleophile compared to DFP). Altogether, this allows us to speculate that less efficient solvation of cations might be the reason for the slightly lower colloidal stability of inks in DFP than in PC. Thus, we propose that the stability of the inks in DFP could be further improved by adding a small amount of a high DN solvent such as DMF or hexamethylphosphoramide.[14]

CONCLUSIONS

In this work, we compared the colloidal stability of PbS-$MAPbI_3$ inks in PC and DFP and studied the effect of aging on their optical properties and electronic transport in FETs. We found that the position of the absorption of the first excitonic peak and its optical density remain stable in both samples for more than 3 months. The PL lifetime of the inks in PC does not deteriorate for over 18 months of storage and remains above 3 μs, while for the inks in DFP, the lifetime initially drops from 3 to 2 μs and then stays at this level even for up to 14 months. For both inks, we observed the appearance of a low-energy PL peak, which we believe is due to a small degree of CQD merging in solution. The presence of chain-like branched CQD aggregates in the inks was confirmed by SAXS analysis. Further evidence of the stability of the PC-based inks was obtained with the fabrication of well-performing FETs with 17-month-old inks with an average electron mobility of 5.2×10^{-3} cm^2/V s. Finally, we speculate that less efficient solvation of cations is the reason for lower colloidal stability of inks in DFP than in PC. We propose that co-solvents with higher Lewis basicity may increase the stability of PbS-$MAPbI_3$ in DFP.

EXPERIMENTAL SECTION

Synthesis of PbS CQDs and Preparation of the Inks. The synthesis and the purification of oleate-capped PbS CQDs were performed as described elsewhere except for the amount of OA (56 mL instead of 70 mL) and injection temperature (80 °C instead of 150 °C).[48] Obtained CQDs have been washed three times by precipitation/redissolution with ethanol/hexane. Washing cycles have been performed in air, but the final pellet after the third cycle has been redissolved in anhydrous hexane and stored in glovebox. Solution-phase ligand exchange was performed by using a modified method.[30] In a typical procedure, 10 mL of NMF solution of 50 mM $MAPbI_3$ solution was combined with 10 mL of oleate-capped PbS CQDs in hexanes with a concentration of 5 mg/mL. The mixture was stirred by using a magnetic stirrer until all the CQDs are transferred into the polar phase. Then, the top phase is discarded and the bottom phase is washed thrice with hexanes. After that, the ligand-exchanged CQDs were immediately precipitated by addition of acetone and collected by centrifugation. The supernatant was discarded, and the pellet was redispersed in the chosen solvent at a concentration of 50−100 mg/mL.

Absorbance and PL Measurements. Diluted inks for absorbance and PL measurements were placed into quartz cuvettes inside a N_2-filled glovebox and sealed with a PTFE cap. The cuvettes were then transferred and stored in ambient atmosphere. Absorption spectra were recorded using a dual-beam Shimadzu UV-3600 spectrometer.

PL spectra were measured by exciting the sample with the second harmonic (400 nm) of a Ti:sapphire laser (Coherent, Mira 900, repetition rate 76 MHz). The emission was spectrally dispersed in a monochromator with a diffraction grating of 30 lines/mm and recorded by a cooled array detector (Andor, iDus 1.7 μm). The excitation beam was spatially limited by an iris and focused with a lens of 150 mm focal length. The fluence was adjusted using gray filters, and spectra were taken in reflection geometry to minimize reabsorption effects. All spectra were corrected for the response of the setup obtained using a calibrated lamp. Time-resolved traces were taken with a Hamamatsu streak camera working in a single sweep mode. An optical pulse selector was used to vary the repetition rate of the exciting pulses.

https://dx.doi.org/10.1021/acsami.0c16646
ACS Appl. Mater. Interfaces 2020, 12, 52959−52966

SAXS Measurements. SAXS measurements have been performed at the MINA instrument at the University of Groningen. The instrument is built on a Cu rotating anode providing high flux collimated X-ray beam of the wavelength 0.154 nm. SAXS patterns have been collected using a two-dimensional Vantec 500 Bruker detector placed 30 cm away from the sample. In order to obtain the 1D SAXS profiles, the SAXS images were radially averaged around the beam center. The sample-to-detector distance and the beam center position have been calibrated using the position of known low-angle diffraction peaks from a standard silver behenate powder. Samples were contained into 1.5 mm flame-sealed capillaries. The scattering from the solvent was removed by subtraction after proper correction for sample absorption. All data manipulation steps were performed using a Matlab software.

The SAXS curves for the CQDs with native OA were fitted using a standard equation for a dilute ensemble of spherical nanoparticles of average radius R with a size distribution $D(R)$

$$I(q)_{\text{sphere}} = I(0)\int_0^{r>2R} P(q, r)D(r)\mathrm{d}r \tag{1}$$

with

$$P(q, r) = \left(\frac{4}{3}\pi r^3 3\frac{\sin(qr) - (qr)\cos(qr)}{(qr)^3}\right)^2 \tag{2}$$

and the term

$$I(0) = \cos t\Delta\rho^2 \tag{3}$$

is a proportionality constant that depends on the instrumental settings and the contrast term

$$\Delta\rho = \rho_{\text{particle}} - \rho_{\text{solvent}} \tag{4}$$

with ρ_i being the specific electron densities in the studied system.

For the inks in PC and DFP, we have used a modified version of the Beaucage equation with two structural levels, namely the spherical particles subunits with average radius R_{subunits} and the aggregates of average radius $R_{\text{g,aggregate}}$

$$I(q)_{\text{ink}} = I(q)_{\text{aggregate}} + I(q)_{\text{subunits}} \tag{5}$$

where

$$I(q)_{\text{aggregate}} = G\exp\left(-\frac{q^2 {R_{\text{g,aggregate}}}^2}{3}\right) + B\exp\left(-\frac{q^2 {R_{\text{subunits}}}^2}{3}\right)\left(\frac{[\text{erf}(q, {R_{\text{g,aggregate}}}^2/\sqrt{6}]^3}{q}\right)^P \tag{6}$$

and

$$I(q)_{\text{subunits}} = I(q)_{\text{sphere}} \tag{7}$$

G and B are constants and P is a power law exponent related to the fractal dimension of the aggregates.

PbS CQD Thin Film FET Fabrication and Measurements. The CQD FETs were fabricated on top of highly doped Si substrates covered with a 230 nm thermally grown SiO_2 dielectric. Prepatterned interdigitated electrodes consisting of 10 nm ITO and 30 nm of Au are served as a source and a drain with a channel width of 10 mm and length of 20 μm. The substrates were cleaned by sonication in acetone and isopropanol, dried in the oven, and treated with O_2-plasma prior the film deposition. The CQD inks in PC and DFP was deposited onto the substrates by blade-coating. FETs were washed with MeOH for 3 min and annealed for 20 min at 120 °C, according to the previously published work.[30] All transistor measurements were performed with an Agilent E5262A semiconductor parameter analyzer. All fabrication and measurement steps were performed in a N_2-filled gloveboxes with O_2 and H_2O concentrations below 0.1 ppm. The hole and electron mobility values were extracted from the transfer (I_D–V_G) characteristics of the FETs in the linear regime using the gradual channel approximation and the parallel plate capacitance of the oxide layer.[49]

■ ASSOCIATED CONTENT

Supporting Information

The Supporting Information is available free of charge at https://pubs.acs.org/doi/10.1021/acsami.0c16646.

Additional absorption spectra, PL decays and spectra, and FET data (PDF)

■ AUTHOR INFORMATION

Corresponding Author

Maria A. Loi − *Zernike Institute for Advanced Materials, University of Groningen, Groningen 9747AG, The Netherlands;* orcid.org/0000-0002-7985-7431; Email: m.a.loi@rug.nl

Authors

Dmytro Bederak − *Zernike Institute for Advanced Materials, University of Groningen, Groningen 9747AG, The Netherlands*

Nataliia Sukharevska − *Zernike Institute for Advanced Materials, University of Groningen, Groningen 9747AG, The Netherlands*

Simon Kahmann − *Zernike Institute for Advanced Materials, University of Groningen, Groningen 9747AG, The Netherlands;* orcid.org/0000-0001-7784-5333

Mustapha Abdu-Aguye − *Zernike Institute for Advanced Materials, University of Groningen, Groningen 9747AG, The Netherlands*

Herman Duim − *Zernike Institute for Advanced Materials, University of Groningen, Groningen 9747AG, The Netherlands*

Dmitry N. Dirin − *Department of Chemistry and Applied Biosciences, ETH Zürich, Zürich 8093, Switzerland; Empa-Swiss Federal Laboratories for Materials Science and Technology, Dübendorf 8600, Switzerland*

Maksym V. Kovalenko − *Department of Chemistry and Applied Biosciences, ETH Zürich, Zürich 8093, Switzerland; Empa-Swiss Federal Laboratories for Materials Science and Technology, Dübendorf 8600, Switzerland;* orcid.org/0000-0002-6396-8938

Giuseppe Portale − *Zernike Institute for Advanced Materials, University of Groningen, Groningen 9747AG, The Netherlands;* orcid.org/0000-0002-4903-3159

Complete contact information is available at: https://pubs.acs.org/10.1021/acsami.0c16646

Notes

The authors declare no competing financial interest.

■ ACKNOWLEDGMENTS

The authors are thankful to A. Kamp and T. Zaharia for the technical support. The Groningen team is grateful for the financial support of the Dieptestrategie program from Zernike Institute for Advanced Materials. M.A.L. and N.S. are grateful for the financial support of the European Research Council via a Starting Grant (HySPOD, no. 306983). S.K. acknowledges the Deutsche Forschungsgemeinschaft (DFG) for a postdoctoral research fellowship (grant number 408012143).

REFERENCES

(1) Kovalenko, M. V.; Manna, L.; Cabot, A.; Hens, Z.; Talapin, D. V.; Kagan, C. R.; Klimov, V. I.; Rogach, A. L.; Reiss, P.; Milliron, D. J.; Guyot-Sionnnest, P.; Konstantatos, G.; Parak, W. J.; Hyeon, T.; Korgel, B. A.; Murray, C. B.; Heiss, W. Prospects of Nanoscience with Nanocrystals. *ACS Nano* **2015**, *9*, 1012−1057.

(2) Ganesan, A.; Houtepen, A.; Crisp, R. Quantum Dot Solar Cells: Small Beginnings Have Large Impacts. *Appl. Sci.* **2018**, *8*, 1867.

(3) Pradhan, S.; Di Stasio, F.; Bi, Y.; Gupta, S.; Christodoulou, S.; Stavrinadis, A.; Konstantatos, G. High-Efficiency Colloidal Quantum Dot Infrared Light-Emitting Diodes via Engineering at the Supra-Nanocrystalline Level. *Nat. Nanotechnol.* **2019**, *14*, 72−79.

(4) Schornbaum, J.; Zakharko, Y.; Held, M.; Thiemann, S.; Gannott, F.; Zaumseil, J. Light-Emitting Quantum Dot Transistors: Emission at High Charge Carrier Densities. *Nano Lett.* **2015**, *15*, 1822−1828.

(5) Shulga, A. G.; Kahmann, S.; Dirin, D. N.; Graf, A.; Zaumseil, J.; Kovalenko, M. V.; Loi, M. A. Electroluminescence Generation in PbS Quantum Dot Light-Emitting Field-Effect Transistors with Solid-State Gating. *ACS Nano* **2018**, *12*, 12805−12813.

(6) Shulga, A. G.; Derenskyi, V.; Salazar-Rios, J. M.; Dirin, D. N.; Fritsch, M.; Kovalenko, M. V.; Scherf, U.; Loi, M. A. An All-Solution-Based Hybrid CMOS-Like Quantum Dot/Carbon Nanotube Inverter. *Adv. Mater.* **2017**, *29*, 1701764.

(7) Mcdonald, S. A.; Konstantatos, G.; Zhang, S.; Cyr, P. W.; Klem, E. J. D.; Levina, L.; Sargent, E. H. Solution-Processed PbS Quantum Dot Infrared Photodetectors and Photovoltaics. *Nat. Mater.* **2005**, *4*, 138−142.

(8) Beygi, H.; Sajjadi, S. A.; Babakhani, A.; Young, J. F.; van Veggel, F. C. J. M. Solution Phase Surface Functionalization of PbS Nanoparticles with Organic Ligands for Single-Step Deposition of p-Type Layer of Quantum Dot Solar Cells. *Appl. Surf. Sci.* **2018**, *459*, 562−571.

(9) Fischer, A.; Rollny, L.; Pan, J.; Carey, G. H.; Thon, S. M.; Hoogland, S.; Voznyy, O.; Zhitomirsky, D.; Kim, J. Y.; Bakr, O. M.; Sargent, E. H. Directly Deposited Quantum Dot Solids Using a Colloidally Stable Nanoparticle Ink. *Adv. Mater.* **2013**, *25*, 5742−5749.

(10) Kovalenko, M. V.; Scheele, M.; Talapin, D. V. Colloidal Nanocrystals with Molecular Metal Chalcogenide Surface Ligands. *Science* **2009**, *324*, 1417−1420.

(11) Fafarman, A. T.; Koh, W.-k.; Diroll, B. T.; Kim, D. K.; Ko, D.-K.; Oh, S. J.; Ye, X.; Doan-Nguyen, V.; Crump, M. R.; Reifsnyder, D. C.; Murray, C. B.; Kagan, C. R. Thiocyanate-Capped Nanocrystal Colloids: Vibrational Reporter of Surface Chemistry and Solution-Based Route to Enhanced Coupling in Nanocrystal Solids. *J. Am. Chem. Soc.* **2011**, *133*, 15753−15761.

(12) Nag, A.; Kovalenko, M. V.; Lee, J.-S.; Liu, W.; Spokoyny, B.; Talapin, D. V. Metal-free Inorganic Ligands for Colloidal Nanocrystals: S2-, HS-, Se2-, HSe-, Te2-, HTe-, TeS32-, OH-, and NH2-as Surface Ligands. *J. Am. Chem. Soc.* **2011**, *133*, 10612−10620.

(13) Tang, J.; Kemp, K. W.; Hoogland, S.; Jeong, K. S.; Liu, H.; Levina, L.; Furukawa, M.; Wang, X.; Debnath, R.; Cha, D.; Chou, K. W.; Fischer, A.; Amassian, A.; Asbury, J. B.; Sargent, E. H. Colloidal-Quantum-Dot Photovoltaics Using Atomic-Ligand Passivation. *Nat. Mater.* **2011**, *10*, 765−771.

(14) Dirin, D. N.; Dreyfuss, S.; Bodnarchuk, M. I.; Nedelcu, G.; Papagiorgis, P.; Itskos, G.; Kovalenko, M. V. Lead Halide Perovskites and Other Metal Halide Complexes As Inorganic Capping Ligands for Colloidal Nanocrystals. *J. Am. Chem. Soc.* **2014**, *136*, 6550−6553.

(15) Zhang, H.; Jang, J.; Liu, W.; Talapin, D. V. Colloidal Nanocrystals with Inorganic Halide, Pseudohalide, and Halometallate Ligands. *ACS Nano* **2014**, *8*, 7359−7369.

(16) Sayevich, V.; Gaponik, N.; Plötner, M.; Kruszynska, M.; Gemming, T.; Dzhagan, V. M.; Akhavan, S.; Zahn, D. R. T.; Demir, H. V.; Eychmüller, A. Stable Dispersion of Iodide-Capped PbSe Quantum Dots for High-Performance Low-Temperature Processed Electronics and Optoelectronics. *Chem. Mater.* **2015**, *27*, 4328−4337.

(17) Ning, Z.; Voznyy, O.; Pan, J.; Hoogland, S.; Adinolfi, V.; Xu, J.; Li, M.; Kirmani, A. R.; Sun, J.-P.; Minor, J.; Kemp, K. W.; Dong, H.; Rollny, L.; Labelle, A.; Carey, G.; Sutherland, B.; Hill, I.; Amassian, A.; Liu, H.; Tang, J.; Bakr, O. M.; Sargent, E. H. Air-Stable n-Type Colloidal Quantum Dot Solids. *Nat. Mater.* **2014**, *13*, 822−828.

(18) Bederak, D.; Balazs, D. M.; Sukharevska, N. V.; Shulga, A. G.; Abdu-Aguye, M.; Dirin, D. N.; Kovalenko, M. V.; Loi, M. A. Comparing Halide Ligands in PbS Colloidal Quantum Dots for Field-Effect Transistors and Solar Cells. *ACS Appl. Nano Mater.* **2018**, *1*, 6882−6889.

(19) Chuang, C.-H. M.; Brown, P. R.; Bulović, V.; Bawendi, M. G. Improved Performance and Stability in Quantum Dot Solar Cells through Band Alignment Engineering. *Nat. Mater.* **2014**, *13*, 796−801.

(20) Jean, J.; Xiao, J.; Nick, R.; Moody, N.; Nasilowski, M.; Bawendi, M.; Bulović, V. Synthesis Cost Dictates the Commercial Viability of Lead Sulfide and Perovskite Quantum Dot Photovoltaics. *Energy Environ. Sci.* **2018**, *11*, 2295−2305.

(21) Liu, M.; Voznyy, O.; Sabatini, R.; García de Arquer, F. P.; Munir, R.; Balawi, A. H.; Lan, X.; Fan, F.; Walters, G.; Kirmani, A. R.; Hoogland, S.; Laquai, F.; Amassian, A.; Sargent, E. H. Hybrid Organic-Inorganic Inks Flatten the Energy Landscape in Colloidal Quantum Dot Solids. *Nat. Mater.* **2017**, *16*, 258−263.

(22) Zhang, X.; Zhang, J.; Phuyal, D.; Du, J.; Tian, L.; Öberg, V. A.; Johansson, M. B.; Cappel, U. B.; Karis, O.; Liu, J.; Rensmo, H.; Boschloo, G.; Johansson, E. M. J. Inorganic $CsPbI_3$ Perovskite Coating on PbS Quantum Dot for Highly Efficient and Stable Infrared Light Converting Solar Cells. *Adv. Energy Mater.* **2017**, *8*, 1702049.

(23) Xu, J.; Voznyy, O.; Liu, M.; Kirmani, A. R.; Walters, G.; Munir, R.; Abdelsamie, M.; Proppe, A. H.; Sarkar, A.; García de Arquer, F. P.; Wei, M.; Sun, B.; Liu, M.; Ouellette, O.; Quintero-Bermudez, R.; Li, J.; Fan, J.; Quan, L.; Todorovic, P.; Tan, H.; Hoogland, S.; Kelley, S. O.; Stefik, M.; Amassian, A.; Sargent, E. H. 2D Matrix Engineering for Homogeneous Quantum Dot Coupling in Photovoltaic Solids. *Nat. Nanotechnol.* **2018**, *13*, 456−462.

(24) Gu, M.; Wang, Y.; Yang, F.; Lu, K.; Xue, Y.; Wu, T.; Fang, H.; Zhou, S.; Zhang, Y.; Ling, X.; Xu, Y.; Li, F.; Yuan, J.; Loi, M. A.; Liu, Z.; Ma, W. Stable PbS Quantum Dot Ink for Efficient Solar Cells by Solution-Phase Ligand Engineering. *J. Mater. Chem. A* **2019**, *7*, 15951−15959.

(25) Choi, H.; Lee, J.-G.; Mai, X. D.; Beard, M. C.; Yoon, S. S.; Jeong, S. Supersonically Spray-Coated Colloidal Quantum Dot Ink Solar Cells. *Sci. Rep.* **2017**, *7*, 622.

(26) Notario, R.; Abboud, J.-L. M. Critical Compilation of Scales of Solvent Parameters. Part I. Pure, Non-Hydrogen Bond Donor Solvents. *Pure Appl. Chem.* **1999**, *71*, 645−718.

(27) Lin, Q.; Yun, H. J.; Liu, W.; Song, H.-J.; Makarov, N. S.; Isaienko, O.; Nakotte, T.; Chen, G.; Luo, H.; Klimov, V. I.; Pietryga, J. M. Phase-Transfer Ligand Exchange of Lead Chalcogenide Quantum Dots for Direct Deposition of Thick, Highly Conductive Films. *J. Am. Chem. Soc.* **2017**, *139*, 6644−6653.

(28) Yang, Z.; Fan, J. Z.; Proppe, A. H.; de Arquer, F. P. G.; Rossouw, D.; Voznyy, O.; Lan, X.; Liu, M.; Walters, G.; Quintero-Bermudez, R.; Sun, B.; Hoogland, S.; Botton, G. A.; Kelley, S. O.; Sargent, E. H. Mixed-Quantum-Dot Solar Cells. *Nat. Commun.* **2017**, *8*, 1325.

(29) Kirmani, A. R.; García de Arquer, F. P.; Fan, J. Z.; Khan, J. I.; Walters, G.; Hoogland, S.; Wehbe, N.; Said, M. M.; Barlow, S.; Laquai, F.; Marder, S. R.; Sargent, E. H.; Amassian, A. Molecular Doping of the Hole-Transporting Layer for Efficient, Single-Step-Deposited Colloidal Quantum Dot Photovoltaics. *ACS Energy Lett.* **2017**, *2*, 1952−1959.

(30) Balazs, D. M.; Rizkia, N.; Fang, H.-H.; Dirin, D. N.; Momand, J.; Kooi, B. J.; Kovalenko, M. V.; Loi, M. A. Colloidal Quantum Dot Inks for Single-Step-Fabricated Field-Effect Transistors: The Importance of Postdeposition Ligand Removal. *ACS Appl. Mater. Interfaces* **2018**, *10*, 5626−5632.

(31) Omogo, B.; Aldana, J. F.; Heyes, C. D. Radiative and Nonradiative Lifetime Engineering of Quantum Dots in Multiple

https://dx.doi.org/10.1021/acsami.0c16646
ACS Appl. Mater. Interfaces 2020, 12, 52959−52966

Solvents by Surface Atom Stoichiometry and Ligands. *J. Phys. Chem. C* **2013**, *117*, 2317−2327.
(32) Portale, G.; Longo, A. Small-Angle X-Ray Scattering for the Study of Nanostructures and Nanostructured Materials. In *Characterization of Semiconductor Heterostructures and Nanostructures*; Elsevier, 2013; pp 175−228.
(33) Longo, A.; Giordano, F.; Giannici, F.; Martorana, A.; Portale, G.; Ruggirello, A.; Turco Liveri, V. Combined Small-Angle x-Ray Scattering/Extended x-Ray Absorption Fine Structure Study of Coated Co Nanoclusters in Bis(2-Ethylhexyl)Sulfosuccinate. *J. Appl. Phys.* **2009**, *105*, 114308.
(34) Jiao, Y.; Akcora, P. Understanding the Role of Grafted Polystyrene Chain Conformation in Assembly of Magnetic Nanoparticles. *Phys. Rev. E* **2014**, *90*, 042601.
(35) Yang, Z.; Janmohamed, A.; Lan, X.; García de Arquer, F. P.; Voznyy, O.; Yassitepe, E.; Kim, G.-H.; Ning, Z.; Gong, X.; Comin, R.; Sargent, E. H. Colloidal Quantum Dot Photovoltaics Enhanced by Perovskite Shelling. *Nano Lett.* **2015**, *15*, 7539−7543.
(36) Yang, Z.; Fan, J. Z.; Proppe, A. H.; De Arquer, F. P. G.; Rossouw, D.; Voznyy, O.; Lan, X.; Liu, M.; Walters, G.; Quintero-Bermudez, R.; Sun, B.; Hoogland, S.; Botton, G. A.; Kelley, S. O.; Sargent, E. H. Mixed-Quantum-Dot Solar Cells. *Nat. Commun.* **2017**, *8*, 1325.
(37) Hwang, G. W.; Kim, D.; Cordero, J. M.; Wilson, M. W. B.; Chuang, C.-H. M.; Grossman, J. C.; Bawendi, M. G. Identifying and Eliminating Emissive Sub-Bandgap States in Thin Films of PbS Nanocrystals. *Adv. Mater.* **2015**, *27*, 4481−4486.
(38) Gilmore, R. H.; Liu, Y.; Shcherbakov-Wu, W.; Dahod, N. S.; Lee, E. M. Y.; Weidman, M. C.; Li, H.; Jean, J.; Bulović, V.; Willard, A. P.; Grossman, J. C.; Tisdale, W. A. Epitaxial Dimers and Auger-Assisted Detrapping in PbS Quantum Dot Solids. *Matter* **2019**, *1*, 250−265.
(39) Zhitomirsky, D.; Furukawa, M.; Tang, J.; Stadler, P.; Hoogland, S.; Voznyy, O.; Liu, H.; Sargent, E. H. N-Type Colloidal-Quantum-Dot Solids for Photovoltaics. *Adv. Mater.* **2012**, *24*, 6181−6185.
(40) Balazs, D. M.; Nugraha, M. I.; Bisri, S. Z.; Sytnyk, M.; Heiss, W.; Loi, M. A. Reducing Charge Trapping in PbS Colloidal Quantum Dot Solids. *Appl. Phys. Lett.* **2014**, *104*, 112104.
(41) Chung, D. S.; Lee, J.-S.; Huang, J.; Nag, A.; Ithurria, S.; Talapin, D. V. Low Voltage, Hysteresis Free, and High Mobility Transistors from All-Inorganic Colloidal Nanocrystals. *Nano Lett.* **2012**, *12*, 1813−1820.
(42) Nugraha, M. I.; Häusermann, R.; Bisri, S. Z.; Matsui, H.; Sytnyk, M.; Heiss, W.; Takeya, J.; Loi, M. A. High Mobility and Low Density of Trap States in Dual-Solid-Gated PbS Nanocrystal Field-Effect Transistors. *Adv. Mater.* **2015**, *27*, 2107−2112.
(43) Reichardt, C. Solvatochromic Dyes as Solvent Polarity Indicators. *Chem. Rev.* **1994**, *94*, 2319−2358.
(44) Taft, R. W.; Pienta, N. J.; Kamlet, M. J.; Arnett, E. M. Linear Solvation Energy Relationships. 7. Correlations between the Solvent-Donicity and Acceptor-Number Scales and the Solvatochromic Parameters .Pi.*, .Alpha., and .Beta. *J. Org. Chem.* **1981**, *46*, 661−667.
(45) Abboud, J.-L. M.; Notari, R. Critical Compilation of Scales of Solvent Parameters. Part I. Pure, Non-Hydrogen Bond Donor Solvents. *Pure Appl. Chem.* **1999**, *71*, 645−718.
(46) Marcus, Y. The Effectivity of Solvents as Electron Pair Donors. *J. Solution Chem.* **1984**, *13*, 599−624.
(47) Stiefvater, O. L.; Lui, S.; Ladd, J. A. The Microwave Spectrum of 2,6-Difluoropyridine. *Z. Naturforsch., A: Phys., Phys. Chem., Kosmophys.* **1976**, *31*, 53−60.
(48) Yarema, M.; Yarema, O.; Lin, W. M. M.; Volk, S.; Yazdani, N.; Bozyigit, D.; Wood, V. Upscaling Colloidal Nanocrystal Hot-Injection Syntheses via Reactor Underpressure. *Chem. Mater.* **2017**, *29*, 796−803.
(49) Bisri, S. Z.; Piliego, C.; Gao, J.; Loi, M. A. Outlook and Emerging Semiconducting Materials for Ambipolar Transistors. *Adv. Mater.* **2014**, *26*, 1176−1199.

https://dx.doi.org/10.1021/acsami.0c16646
ACS Appl. Mater. Interfaces 2020, 12, 52959−52966